Gruppo Italiano Frattura (IGF)
Atti III Convegno Nazionale
Torino, 22-23 maggio 1986

UN APPROCCIO DI TEORIA DELLE CATASTROFI ALLA MECCANICA DELLA FRATTURA

Alberto Carpinteri
Istituto di Scienza delle Costruzioni, Università di Bologna, 40136 Bologna.

Sommario

Si utilizza un modello di crack coesivo per l'analisi della stabilità di fessure in materiali elasto-softening. La forma della curva di risposta carico-spostamento varia notevolmente al variare della scala dimensionale e mantenendo invariata la forma geometrica della struttura. Il ramo discendente diviene sempre più ripido all'aumentare della scala dimensionale. Esiste poi una dimensione critica per cui la pendenza del ramo discendente è infinita.
In questo caso la capacità di carico diminuisce drasticamente per incrementi di deformazione relativamente piccoli.Per dimensioni maggiori, quindi, la pendenza diventa positiva e appare una cuspide nella curva carico-spostamento.
Si dimostra che tale punto di biforcazione può essere rivelato dalla ben nota condizione di meccanica della frattura elastica lineare: $K_I = K_{IC}$.

A CATASTROPHE THEORY APPROACH TO FRACTURE MECHANICS

Alberto Carpinteri

Istituto di Scienza delle Costruzioni, University of Bologna
40136 Bologna, Italy

ABSTRACT

A cohesive crack model is applied to analyze the crack stability in elastic-softening materials. The shape of the global load-displacement response changes substantially by varying size-scale and keeping geometrical shape of the structure unchanged. The softening branch becomes steeper and steeper when the size-scale increases. A critical size-scale does exist for which the softening slope is infinite. In such a case, the load carrying capacity drastically decreases for relatively small displacement increments. Then, for larger size-scales, the softening slope becomes positive and a cusp catastrophe appears. It is proved that such a bifurcation point can be revealed by the simple LEFM condition $K_I = K_{IC}$.

INTRODUCTION

The Catastrophe Theory was applied by Thompson and Shorrock [1] to demonstrate the existence of a cusp catastrophe in a symmetry-breaking instability of a close packed atomic lattice. This work was then extended to demonstrate the existence of the more complex hyperbolic umbilic catastrophe in a three-dimensional failure stress-locus [2]. More recently, Potier-Ferry [3] gave an interpretation of the Linear Elastic Fracture Mechanics instability in terms of Catastrophe Theory. An attempt is made in this paper to explain the transition from ductile to brittle behaviour when the structure size increases, based on the elementary concepts of Thom's Theory [4]. For relatively large structure sizes, catastrophic jumps may occur when a smooth variation of control variable (displacement) causes a discontinuous change of behaviour variable (load). For relatively small structure sizes, such jumps are not predicted.

A cohesive crack model is applied to analyze the *local* or slow crack growth in elastic-softening materials. The shape of the *global* load-displacement response changes substantially by varying size-scale and keeping geometrical shape of the structure unchanged. The softening branch becomes steeper and steeper when the size-scale increases. A critical size-scale does exist for which the softening slope is

infinite. In such a case the load carrying capacity drastically decreases for relatively small displacement increments. Then, for size-scales larger than the critical one, the softening slope becomes positive and part of the load-displacement path results to be virtual if the loading process is displacement-controlled. In such a case, the loading capacity will present a discontinuity with a negative jump. The size-scale transition from ductile to brittle behaviour is governed by a nondimensional brittleness number s_E which is a function of material properties and structure size-scale. A truly brittle failure occurs only with relatively low fracture toughnesses, $\mathcal{G}_{IC}$, high tensile strengths, σ_u, and/or large structure size-scales, b, i.e., when $s_E = \mathcal{G}_{IC}/\sigma_u b \to 0$.

On the other hand, if the loading process is controlled by a monotonically increasing function of time (e.g., the crack mouth opening displacement or a linear combination of load and displacement), the indentation in the load-displacement curve can be captured experimentally. When the post-peak behaviour is kept under control up to the complete structure separation, the area delimited by load-displacement curve and displacement-axis represents the product of $\mathcal{G}_{IC}$ by the initial ligament area.

Eventually, it is proved that, for $s_E \to 0$, the maximum load of catastrophical failure may be provided by the simple LEFM condition: $K_I = K_{IC} = \sqrt{\mathcal{G}_{IC} E}$ (plane stress), and that slow crack growth and process zone are lacking before the catastrophical event.

COHESIVE CRACK MODELLING

The cohesive crack model is based on the following assumptions [5 - 8].
(1) The cohesive fracture zone (plastic or process zone) begins to develop when the maximum principal stress achieves the ultimate tensile strength σ_u (Figure 1-a).
(2) The material in the process zone is partially damaged but still able to transfer stress. Such a stress is dependent on the crack opening displacement w (Figure 1-b).

The *real crack tip* is defined as the point where the distance between the crack surfaces is equal to the critical value of crack opening displacement w_c and the normal stress vanishes (Figure 2-a). On the other hand, the *fictitious crack tip* is defined as the point where the normal stress attains the maximum value σ_u and the crack opening vanishes (Figure 2-a).

The closing stresses acting on the crack surfaces (Figure 2-a) can be replaced by nodal forces (Figure 2-b). The intensity of these forces depends on the opening of the fictitious crack, w, according to the $\sigma - w$ constitutive law of the material (Figure 1-b). When the tensile strength σ_u is achieved at the fictitious crack tip (Figure 2-b), the top node is opened and a cohesive force starts acting across the crack, while the fictitious crack tip moves to the next node.

With reference to the three point bending test (TPBT) geometry in Figure 3, the nodes are distributed along the potential fracture line. It is impossible to extend the fracture nodes to the whole cross-section depth, as would be required to follow

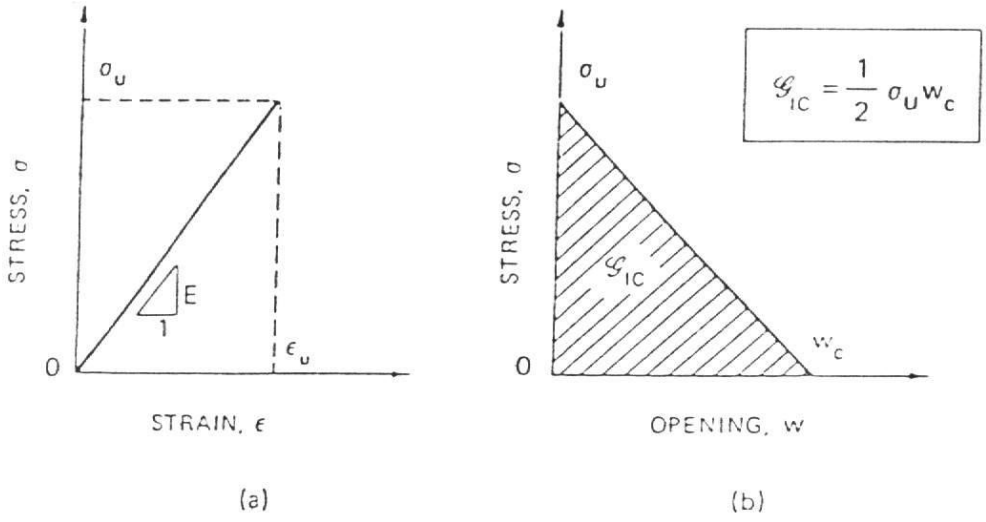

Fig. (1) - Stress-strain (a) and stress-crack opening displacement (b) constitutive laws.

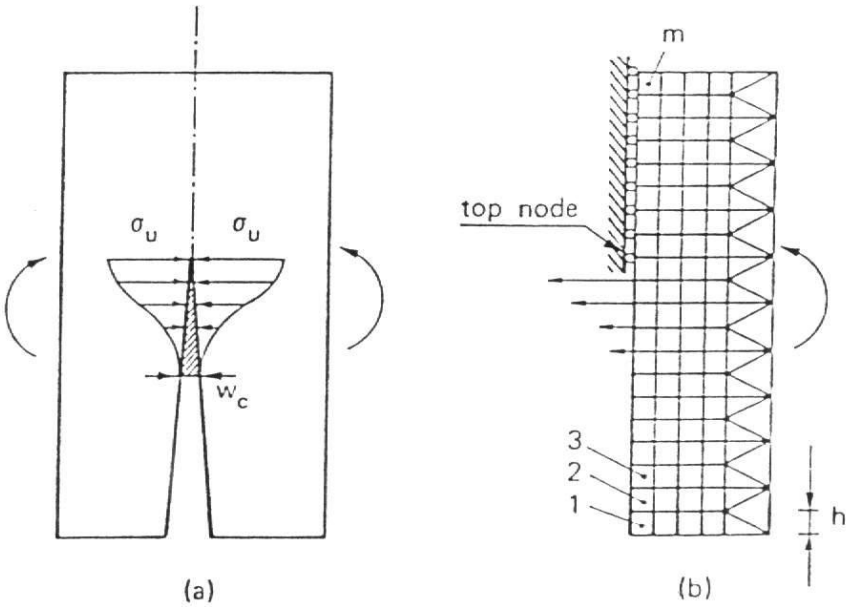

Fig. (2) - Stress distribution across the cohesive zone (a) and equivalent nodal forces in the finite element mesh (b).

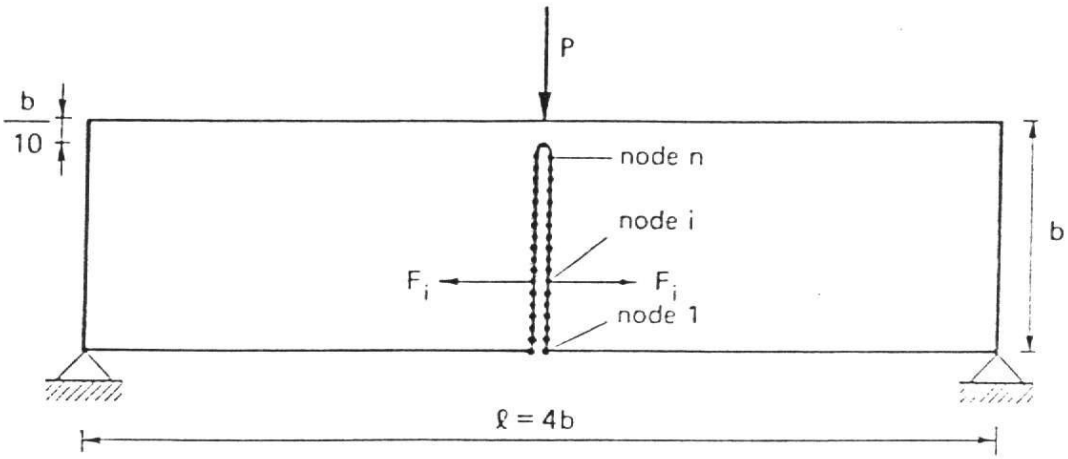

Fig. (3) - Finite element nodes along the potential fracture line.

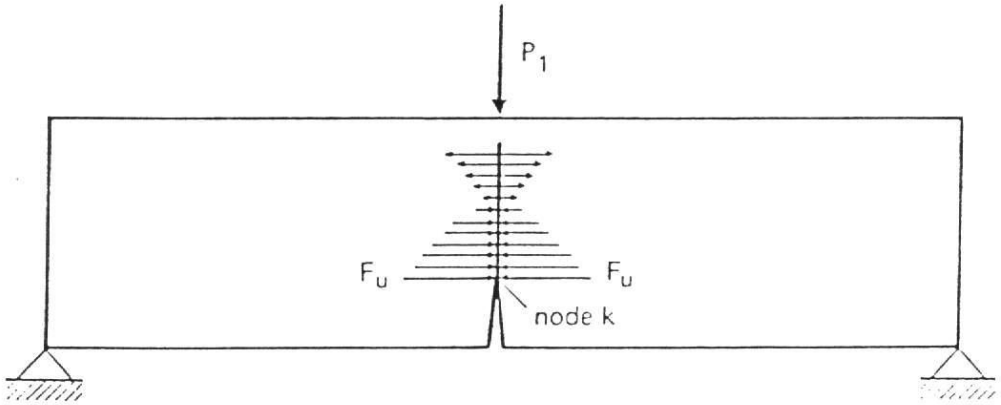

(a)

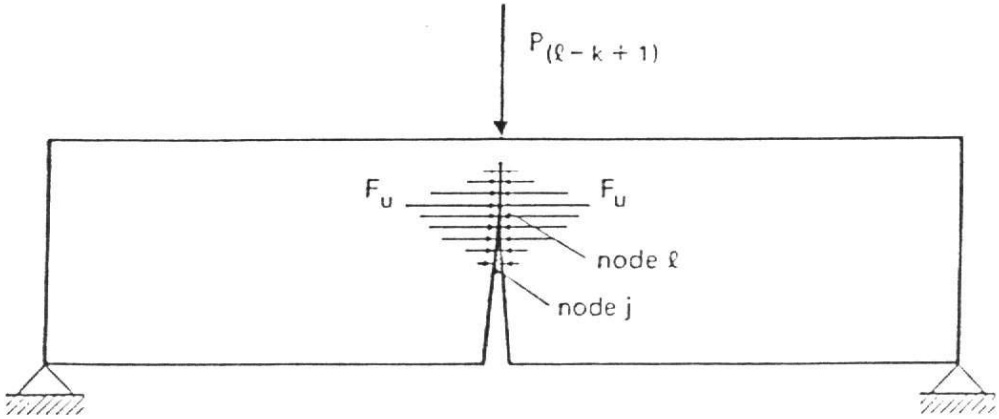

(b)

Fig. (4) - Cohesive crack configurations at the first (a) and (1 - k + 1)-th (b) crack growth increment.

the fracture process up to the complete load relaxation, since a sufficiently large ligament is needed to guarantee a correct structural analysis. A ligament equal to one tenth of the depth (b/10) is assumed.

The coefficients of influence in terms of node openings and deflection are computed by a finite element analysis where the fictitious structure in Figure 3 is subjected to (n + 1) different loading conditions. Consider the TPBT in Figure 4-a with the initial crack tip in the node k. The crack opening displacements at the n fracture nodes may be expressed as follows:

$$\underset{\sim}{\omega} = \underset{\sim}{K}\ \underset{\sim}{F} + \underset{\sim}{C}\ P + \underset{\sim}{\Gamma} \quad , \tag{1}$$

being:

$\underset{\sim}{\omega}$ = vector of the crack opening displacements,

$\underset{\sim}{K}$ = matrix of the coefficients of influence (nodal forces),

$\underset{\sim}{F}$ = vector of the nodal forces,

$\underset{\sim}{C}$ = vector of the coefficients of influence (external load),

P = external load,

$\underset{\sim}{\Gamma}$ = vector of the crack opening displacements due to the specimen weight.

On the other hand, the initial crack is stress-free and therefore:

$$F_i = 0 \quad , \qquad \text{for} \quad i = 1, 2, \ldots, (k-1) \quad , \tag{2-a}$$

while at the ligament there is no displacement discontinuity:

$$\omega_i = 0 \quad , \qquad \text{for} \quad i = k, (k+1), \ldots, n \quad . \tag{2-b}$$

Equations (1) and (2) constitute a linear algebraical system of 2 n equations and 2 n unknowns, i.e. the elements of vectors $\underset{\sim}{\omega}$ and $\underset{\sim}{F}$. If load P and vector $\underset{\sim}{F}$ are known, it is possible to compute the beam deflection, δ :

$$\delta = \underset{\sim}{C}^T\ \underset{\sim}{F} + D_P\ P + D_\gamma \quad , \tag{3}$$

where D_P is the deflection for P = 1 and D_γ is the deflection due to the specimen weight.

After the first step, a cohesive zone forms in front of the real crack tip (Figure 4-b), say between nodes j and l. Then equations (2) are replaced by:

$$F_i = 0 \quad , \qquad \text{for } i = 1, 2, \ldots, (j-1) \quad , \tag{4-a}$$

$$F_i = F_u \left(1 - \frac{\omega_i}{\omega_c}\right), \qquad \text{for } i = j, (j+1), \ldots, l \quad , \tag{4-b}$$

$$\omega_i = 0 \quad , \qquad \text{for } i = l, (l+1), \ldots, n \quad , \tag{4-c}$$

where F_u is the ultimate strength nodal force:

$$F_u = 0.9\, b\, \sigma_u / n \ . \qquad (5)$$

Equations (1) and (4) constitute a linear algebraical system of (2 n + 1) equations and (2 n + 1) unknowns, i.e. the elements of vectors $\underset{\sim}{w}$ and $\underset{\sim}{F}$ and the external load P.

At the first step, the cohesive zone is missing (l = j = k) and the load P_1 producing the ultimate strength nodal force F_u at the initial crack tip (node k) is computed. Such a value P_1, together with the related deflection δ_1 computed through equation (3), gives the first point of the P - δ curve. At the second step the cohesive zone is between the nodes k and (k + 1), and the load P_2 producing the force F_u at the second fictitious crack tip (node k + 1) is computed. Equation (3) then provides the deflection δ_2. At the third step, the fictitious crack tip is in the node (k + 2), and so on. The present numerical program simulates a loading process where the controlling parameter is the fictitious crack depth. On the other hand, real (or stress-free) crack depth, external load and deflection are obtained at each step after an iterative procedure.

The program stops with the untieing of the node n and, consequently, with the determination of the last couple of values F_n and δ_n. In this way, the complete load-deflection curve is automatically plotted by the computer.

SIZE-SCALE TRANSITION FROM DUCTILE TO CATASTROPHICAL FAILURE

Let us consider a cracked beam in flexure with the span, l , equal to four times the beam depth, b , (Figure 5-a). Such sizes will be scaled with geometrical similitude, whereas the beam thickness will be kept constant, t = 10 cm. The initial crack depth, a_o/b, will range between 0.0 (initially uncracked beam) and 0.5. The mechanical properties are those thypical of a concrete-like material:

Young's modulus, E = 400 000 kg/cm^2,
Ultimate tensile strength, σ_u = 40 kg/cm^2 ,
Critical crack opening displacement, w_c = 0.005 cm .

The area under the σ vs. w curve in Figure 1-b is the strain energy release rate $\mathcal{G}_{IC} = \frac{1}{2}\, \sigma_u\, w_c = 0.1$ kg/cm.

For the size-scale parameter b = 10 cm, the load-deflection curves are reported in Figure 6-a by varying the initial crack depth, a_o/b. For deep cracks, stiffness and loading capacity decrease, whereas ductility increases. The slope of the softening branch achieves its maximum when the beam is initially uncracked.

The load-deflection curves in Figure 6-b relate to the case b = 20 cm. The general trend by varying the geometrical ratio a_o/b is the same as in Figure 6-a. In this case, however, the maximum softening slope for a_o/b = 0 is nearly infinite and a drop in the load carrying capacity is predicted when $\delta \simeq 12 \times 10^{-3}$ cm.

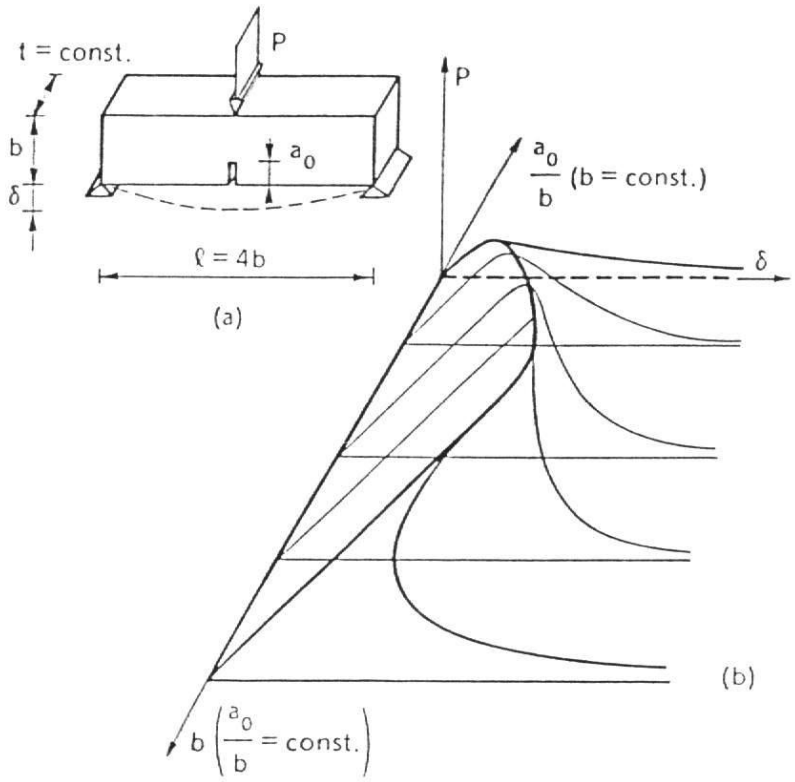

Fig. (5) - Three point bending specimen (a) and catastrophe manifold (b).

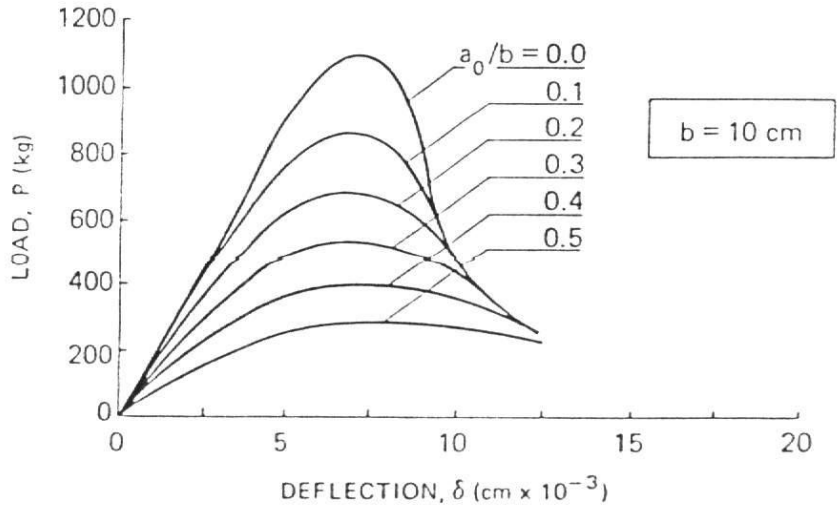

Fig. (6-a)

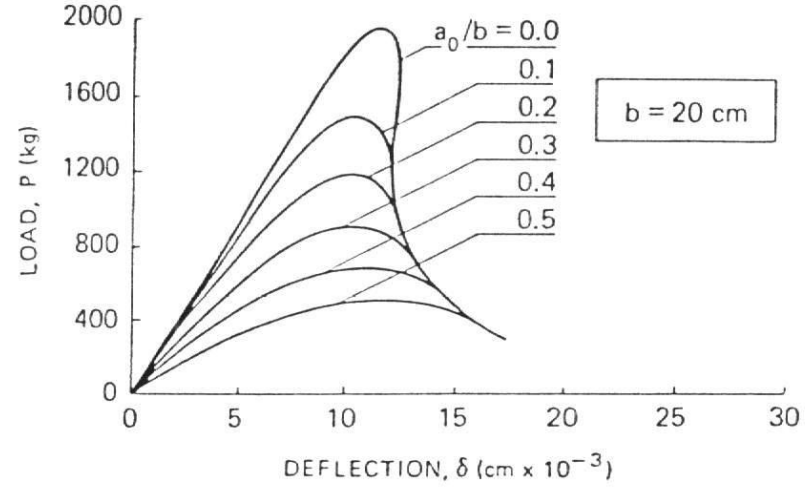

Fig. (6-b)

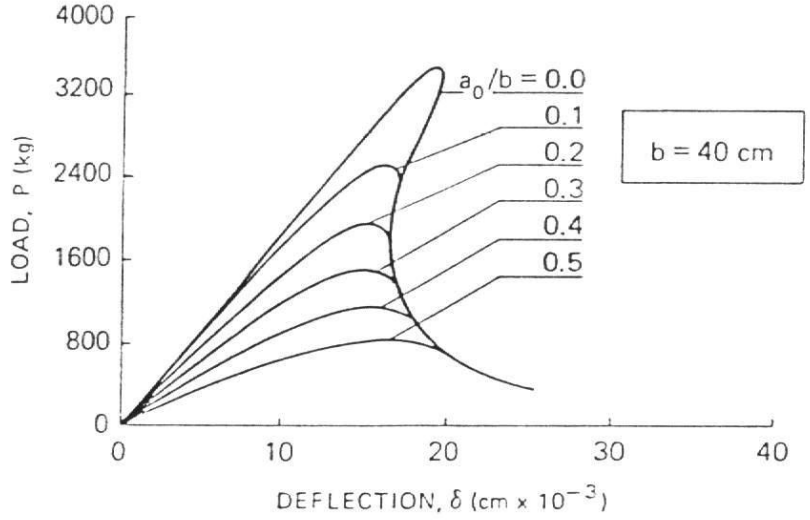

Fig. (6-c)

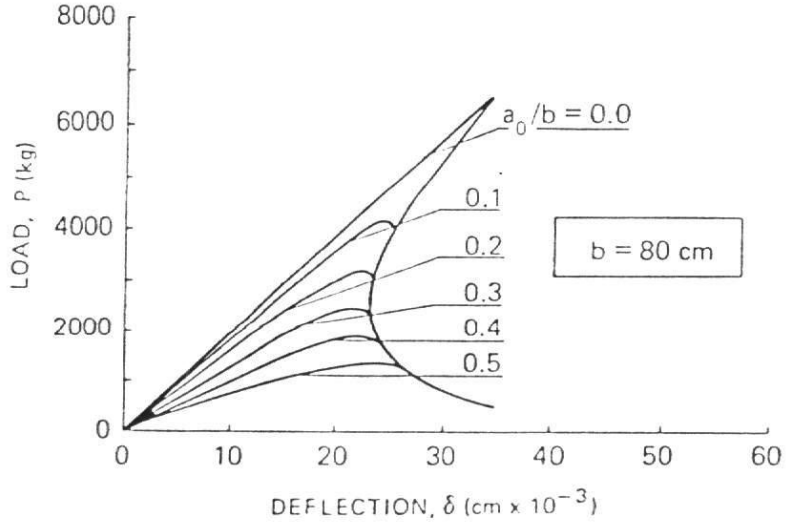

Fig. (6-d)

Fig. (6) - Load-deflection curves by varying the initial crack depth, a_o/b. (a) b = 10 cm; (b) b = 20 cm; (c) b = 40 cm; (d) b = 80 cm.

The case b = 40 cm is described in Figure 6-c. For $a_o/b \lesssim 0.20$, the softening slope presents even positive values with an indenting shape of the P - δ curve. If the loading process is deflection-controlled, the load will present a discontinuity with a negative jump. Substantially, this is the case of a cusp catastrophe.

The case b = 80 cm is eventually contemplated in Figure 6-d. The cusp catastrophe occurs for $a_o/b \lesssim 0.25$. That is, when the size-scale increases, the initial crack depth interval of cusp catastrophe spreads.

The opposite trends of brittleness increase by increasing size-scale and/or decreasing initial crack depth, are shown schematically in Figure 5-b. The gradual transition from simple fold catastrophe to bifurcation or cusp catastrophe generates an equilibrium surface (or catastrophe manifold).

The maximum loading capacity $P^{(1)}_{max}$ according to the cohesive crack model is obtained from the P - δ diagrams in Figures 6. On the other hand, the maximum load $P^{(2)}_{max}$ according to LEFM can be derived from the following formula [9] :

$$P^{(2)}_{max} = \frac{K_{IC}\, t\, b^{3/2}}{l\, f(a_o/b)} \quad , \tag{6}$$

with the shape-function f given by:

$$f\left(\frac{a_o}{b}\right) = 2.9\left(\frac{a_o}{b}\right)^{1/2} - 4.6\left(\frac{a_o}{b}\right)^{3/2} + 21.8\left(\frac{a_o}{b}\right)^{5/2} - 37.6\left(\frac{a_o}{b}\right)^{7/2} + 38.7\left(\frac{a_o}{b}\right)^{9/2}, \tag{7}$$

and the critical value of stress-intensity factor K_{IC} computed according to the well-known relationship:

$$K_{IC} = \sqrt{\mathcal{G}_{IC}\, E} \quad . \tag{8}$$

The values of the ratio $P^{(1)}_{max} / P^{(2)}_{max}$ are reported as functions of the dimensionless size, $b\,\sigma_u / \mathcal{G}_{IC}$, or equivalently, of the brittleness number, $s_E = \mathcal{G}_{IC} / \sigma_u\, b$ [10 - 14] in Figure 7. The ratio $P^{(1)}_{max} / P^{(2)}_{max}$ may also be regarded as the ratio of the fictitious fracture toughness (given by the non-linear maximum load) to the true fracture toughness (considered as a material constant).

It is evident that, for low s_E values, the results of the cohesive crack model tend to those of LEFM [13] :

$$\lim_{s_E \to 0} P^{(1)}_{max} = P^{(2)}_{max} \quad , \tag{9}$$

and, therefore, the maximum loading capacity can be predicted applying the simple condition $K_I = K_{IC}$.

The fictitious crack depth at the maximum load is plotted as a function of the inverse of brittleness number s_E in Figures 8. The brittleness increase for $s_E \to 0$

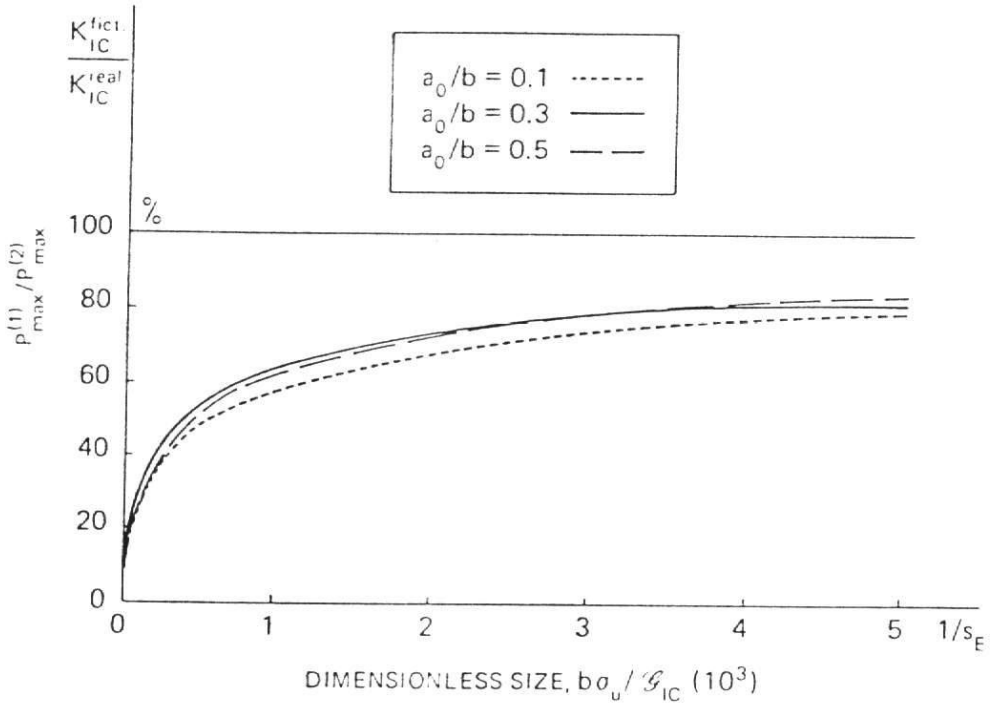

Fig. (7) - Size-scale transition towards LEFM.

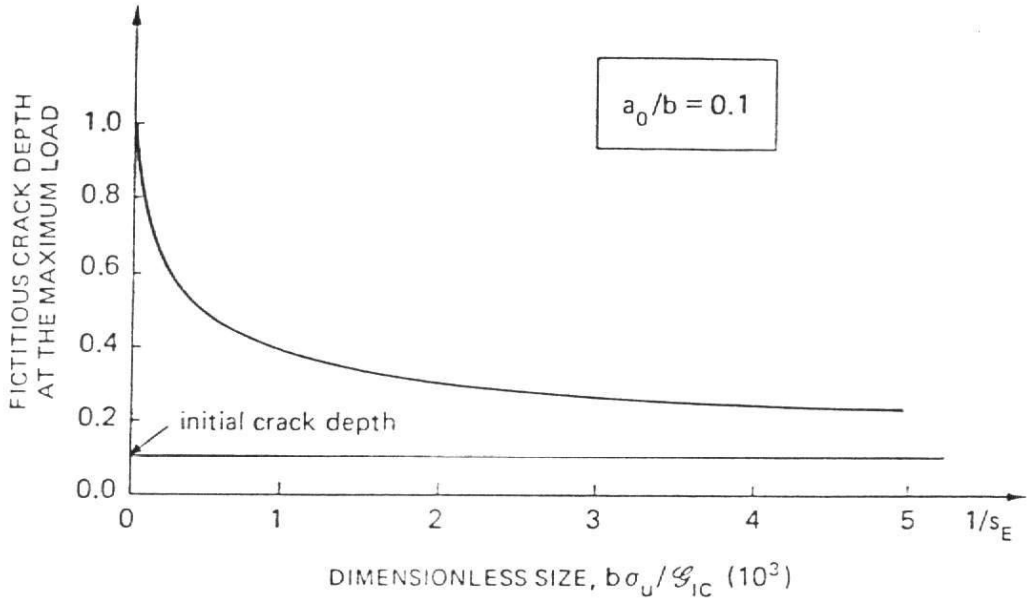
$a_0/b = 0.1$
FICTITIOUS CRACK DEPTH AT THE MAXIMUM LOAD
1.0
0.8
0.6
0.4
0.2
0.0
initial crack depth
0
1
2
3
4
5
$1/s_E$
DIMENSIONLESS SIZE, $b\sigma_u/\mathcal{G}_{IC}$ (10^3)

Fig. (8-a)

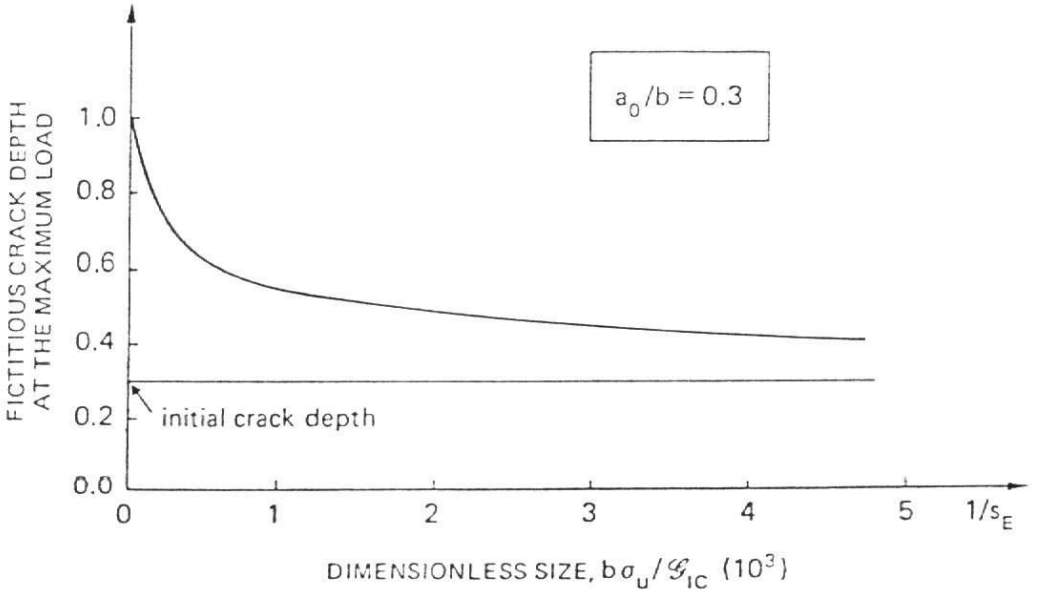
$a_0/b = 0.3$
FICTITIOUS CRACK DEPTH AT THE MAXIMUM LOAD
1.0
0.8
0.6
0.4
0.2
0.0
initial crack depth
0
1
2
3
4
5
$1/s_E$
DIMENSIONLESS SIZE, $b\sigma_u/\mathcal{G}_{IC}$ (10^3)

Fig. (8-b)

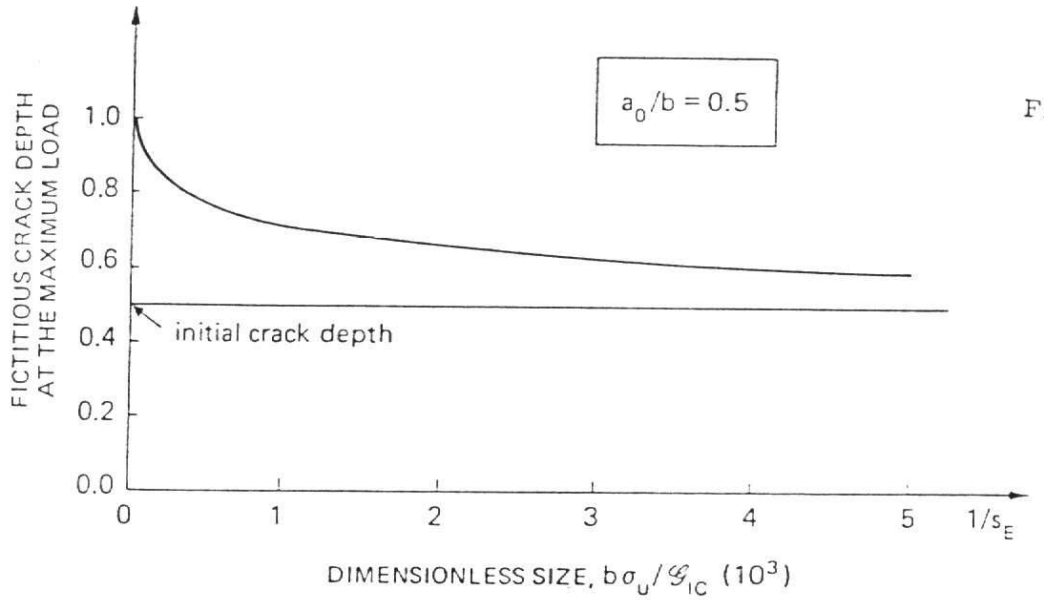

Fig. (8-c)

Fig. (8) - Fictitious crack depth at the maximum load as a function of dimensionless size. (a) $a_o/b = 0.1$; (b) $a_o/b = 0.3$; (c) $a_o/b = 0.5$.

is evident also from these diagrams, the process zone at $dP/d\delta = 0$ tending to disappear, whereas it tends to cover the whole ligament for $s_E \to \infty$ (ductile collapse). The real (or stress-free) crack depth at the maximum load is nearly coincident with the initial crack depth for each value of s_E. This means that the slow crack growth does not start before the softening stage. Therefore, neither the slow crack growth occurs nor the cohesive zone develops before the peak, when $s_E \to 0$(*).

Recalling once again Figures 7 and 8, it is possible to state that, the smaller the brittleness number s_E is, i.e., the lower the fracture toughness $\mathcal{G}_{IC}$, the larger the size-scale b and/or the higher the ultimate tensile strength σ_u, the more accurate the cusp catastrophe is in reproducing the classical LEFM instability [13].

FRACTURE ENERGY DISSIPATION AND BRITTLENESS LIMIT FOR INFINITE SIZE-SCALE

If the loading process is controlled by a monotonically increasing function of time, like, for instance, the crack mouth opening displacement [13] or the linear combination of load and displacement ($\delta \cos\theta - P \sin\theta$), where θ represents a rotation of the control plane δ versus b about the b-axis [15], the indentation or virtual branch of the load-displacement curve can be captured experimentally. When the post-peak behaviour is kept under control up to the complete structure separation, the area delimited by load-displacement curve and displacement-axis represents the product of strain energy release rate, $\mathcal{G}_{IC}$, by the initial ligament area, $(b - a_o)\, t$, (Figures 9). The area under the curve $a_o/b = 0.0$ is thus twice that under the curve $a_o/b = 0.5$ in Figure 6-a, as well as the half of that under the curve $a_o/b = 0.0$ in Figure 6-b, etc. This simple result is due to the assumption that energy dissipation occurs only on the fracture surface, while in reality energy is also dissipated in a damage volume around the crack tip, as shown by Carpinteri and Sih in [16]. On the other hand, the cohesive crack assumption is more than acceptable for slender beams, where bending prevails over shear and the energy dissipation occurs in a very narrow crack band [17].

When the brittleness number $s_E \to 0$, $P^{(1)}_{max} = P^{(2)}_{max}$ and equations (6) and (8) provide:

$$\mathcal{G}_{IC} = P^2_{max} \frac{(1/b)^2 f^2(a_o/b)}{b t^2 E} \quad . \tag{10}$$

In a three point bending specimen of linear elastic material the deflection is given by the contribution of a distributed and a concentrated compliance respectively:

$$\delta = \frac{P}{E t} \left[\frac{1}{4} \left(\frac{l}{b}\right)^3 + \frac{3}{2} \left(\frac{l}{b}\right)^2 g\left(\frac{a_o}{b}\right) \right] , \tag{11}$$

(*) Slow crack growth and cohesive zone may develop only if both load and displacement are decreased, following the virtual branch with positive slope. On the other hand, with normal softening (i.e., only negative slope in the $P - \delta$ curve after the peak) only the load must be decreased to control the fracture process.

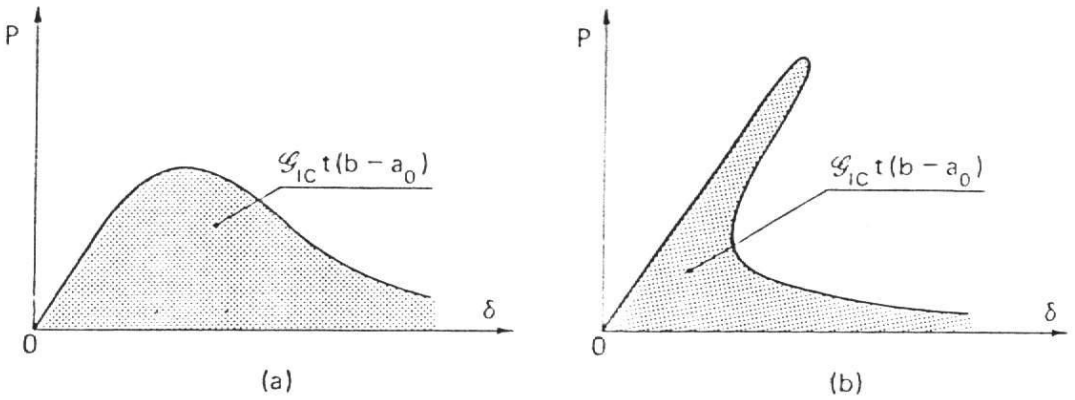

Fig. (9) - Energy dissipated in the fracturing process. Ductile (a) and brittle (b) behaviour.

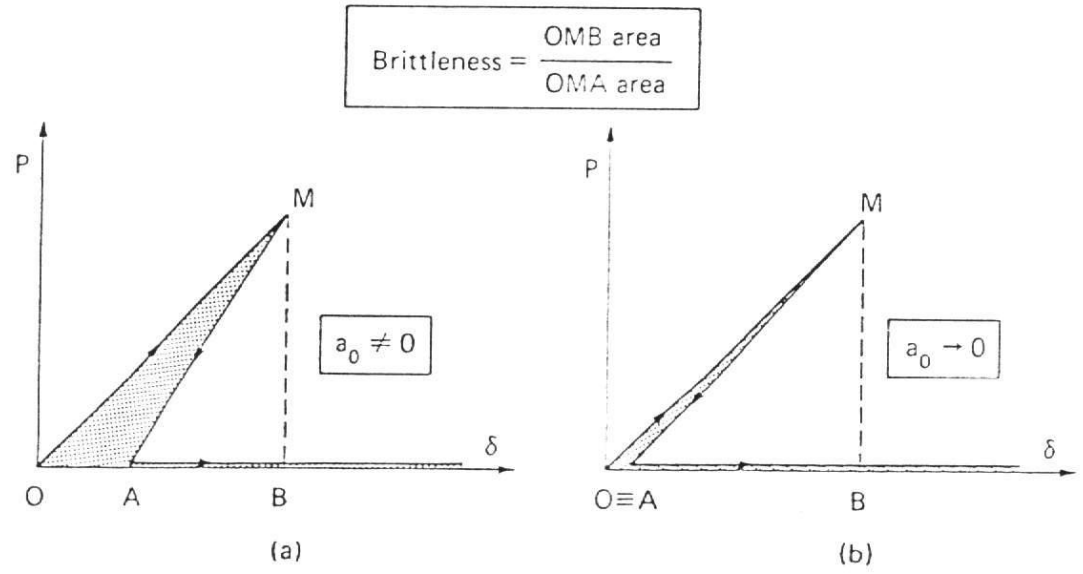

Fig. (10) - Definition of structure brittleness as the ratio of elastic energy contained in the body at the bifurcation point to energy dissipated in the fracturing process. Initially cracked (a) and uncracked (b) specimen.

where [18]:

$$g\left(\frac{a_o}{b}\right) = \left(\frac{a_o/b}{1-\frac{a_o}{b}}\right)^2 \left\{5.58 - 19.57\left(\frac{a_o}{b}\right) + 36.82\left(\frac{a_o}{b}\right)^2 - 34.94\left(\frac{a_o}{b}\right)^3 + 12.77\left(\frac{a_o}{b}\right)^4\right\}. \quad (12)$$

Relation (11) is valid also for the point of instability, and then equation (10) is transformed as follows:

$$\mathcal{G}_{IC}\,(b - a_o)\,t = \left(P_{max}\,\delta_{max}/2\right) \frac{2\,f^2\left(\frac{a_o}{b}\right)\left(1-\frac{a_o}{b}\right)}{\frac{1}{4}\left(\frac{1}{b}\right) + \frac{3}{2}\,g\left(\frac{a_o}{b}\right)}\,. \quad (13)$$

If *Brittleness* is defined as the ratio of the elastic energy contained in the body at the point of instability to the energy which can be dissipated in the body (Figure 10-a), it results to be a function of beam slenderness and initial crack depth:

$$Brittleness = \frac{\frac{1}{2}\,P_{max}\,\delta_{max}}{\mathcal{G}_{IC}\,(b - a_o)\,t} = \frac{\frac{1}{4}\left(\frac{1}{b}\right) + \frac{3}{2}\,g\left(\frac{a_o}{b}\right)}{2\left(1-\frac{a_o}{b}\right) f^2\left(\frac{a_o}{b}\right)}\,. \quad (14)$$

When the beam is initially uncracked, i.e., $a_o/b = 0$, the brittleness tends to infinity and the softening branch is coincident with the elastic one (Figure 10-b). On the other hand, when the initial crack length is different from zero ($a_o \neq 0$), the brittleness tends to the value in equation (14) for the size-scale tending to infinity (Figure 10-a). In this case, the softening branch is always distinct from the elastic one.

When the beam is initially uncracked, the elastic energy contained in the body at the point of instability is an infinite quantity of higher rank with respect to the fracture energy, the former being proportional to $b^3\,(\sigma_u^2/E)$ and the latter to $b^2\,\mathcal{G}_{IC}$. When there is an initial crack, the two quantities are of the same rank for the size-scale b tending to infinity, their ratio being finite and provided in equation (14).

ACKNOWLEDGEMENTS

The numerical results reported in the present paper were obtained in a joint research program between ENEL-CRIS-Milano and the University of Bologna.

REFERENCES

[1] Thompson, J. M. T. and Shorrock, P. A., "Bifurcational instability of an atomic lattice", Journal of Mechanics and Physics of Solids, 23, pp. 21 - 37, 1975.

[2] Thompson, J. M. T. and Shorrock, P. A., "Hyperbolic umbilic catastrophe in crystal fracture", Nature, 260, pp. 598 - 599, 1976.

[3] Potier-Ferry, M., "Towards a catastrophe theory for the mechanics of plasticity and fracture", International Journal of Engineering Science, 23, pp. 821 - 837, 1985.

[4] Thom, R., "Structural Stability and Morphogenesis", Benjamin, New York, 1972.

[5] Hillerborg, A., Modeer, M. and Petersson, P. E., "Analysis of crack formation and crack growth in concrete by means of fracture mechanics and finite elements", Cement and Concrete Research, 6, pp. 773 - 782, 1976.

[6] Petersson, P. E., "Crack growth and development of fracture zones in plain concrete and similar materials", Report TVBM-1006, Division of Building Materials, Lund Institute of Technology, 1981.

[7] Colombo, G. and Limido, E., "Un metodo numerico per l'analisi di prove TPBT stabili: confronto con alcuni dati sperimentali", XI Convegno Nazionale dell'Associazione Italiana per l'Analisi delle Sollecitazioni, Torino, pp. 233 - 243, 1983.

[8] Carpinteri, A., Di Tommaso, A. and Fanelli, M., "Influence of material parameters and geometry on cohesive crack propagation", International Conference on Fracture Mechanics of Concrete, Lausanne, October 1 - 3, 1985.

[9] Standard Method of Test for Plane Strain Fracture Toughness of Metallic Materials, E 399 - 74, ASTM.

[10] Carpinteri, A., "Size effect in fracture toughness testing: a dimensional analysis approach", Proceedings of the International Conference on Analytical and Experimental Fracture Mechanics, June 23 - 27, 1980, Roma, edited by G. C. Sih and M. Mirabile, Sijthoff & Noordhoff, pp. 785 - 797, 1981.

[11] Carpinteri, A., "Notch sensitivity in fracture testing of aggregative materials", Engineering Fracture Mechanics, 16, pp. 467 - 481, 1982.

[12] Carpinteri, A., Marega, C. and Savadori, A., "Ductile-brittle transition by varying structural size", Engineering Fracture Mechanics, 21, pp. 263 - 271, 1985.

[13] Carpinteri, A., "Interpretation of the Griffith instability as a bifurcation of the global equilibrium", Application of Fracture Mechanics to Cementitious Composites, NATO Advanced Research Workshop, September 4 - 7, 1984, Northwestern University, edited by S.P. Shah, Martinus Nijhoff Publishers, pp. 287 - 316, 1985.

[14] Carpinteri, A., "Limit analysis for elastic-softening structures: scale and slenderness influence on the global brittleness", Structure and Crack Propagation in Brittle Matrix Composite Materials, Euromech Colloquium No. 204, November 12 - 15, 1985, Jablonna(Warsaw), edited by A. M. Brandt, Elsevier Applied Science Publishers, in press.

[15] Rokugo, K., Ohno, S. and Koyanagy, W., "Automatical measuring system of load-displace

ment curves including post-failure region of concrete specimens", International Conference on Fracture Mechanics of Concrete, Lausanne, October 1 - 3, 1985.

[16] Carpinteri, A. and Sih, G. C., "Damage accumulation and crack growth in bilinear materials with softening", Theoretical and Applied Fracture Mechanics, 1, pp.145-159, 1984.

[17] Bažant, Z. P. and Cedolin, L., "Blunt crack band propagation in finite element analysis", Journal of the Engineering Mechanics Division, ASCE, 105, pp. 297 - 315, 1979.

[18] Tada, H., Paris, P. and Irwin, G., The Stress Analysis of Cracks Handbook , Del Research Corporation, St. Louis, Missouri, pp. 2·16 - 17, 1963.